JOURNAL OF AIRCRAFT
Vol. 43, No. 3, May–June 2006

Engineering Notes

ENGINEERING NOTES are short manuscripts describing new developments or important results of a preliminary nature. These Notes should not exceed 2500 words (where a figure or table counts as 200 words). Following informal review by the Editors, they may be published within a few months of the date of receipt. Style requirements are the same as for regular contributions (see inside back cover).

Design Exploration of Aerodynamic Wing Shape for Reusable Launch Vehicle Flyback Booster

Kazuhisa Chiba,* Shigeru Obayashi,† and Kazuhiro Nakahashi‡
Tohoku University, Sendai 980-8577, Japan

I. Introduction

A SPACE transportation system with a substantially reduced cost[1] is needed so that space can be utilized in many more fields. For this purpose, research has focused on the reusable launch vehicle (RLV) system,[2] suggested as a replacement for the present expendable launch vehicle (ELV) system. Single-stage-to-orbit (SSTO) launch systems, such as the X-33 (see Ref. 3), have been studied because this configuration is ideal for reuse similar to that of aircraft. However, these studies indicated that the SSTO configuration had difficulties because it would require a higher performance propulsion system and greater reduction of its structure weight than can be attained based on the present technology. Consequently, current proposals for the introduction of reusable components in space transportation involve the two-stage-to-orbit (TSTO) configuration with winged flyback boosters powered by liquid rocket engines[4] for vertical takeoff and horizontal landing (VTHL). For the realization of this configuration, many approaches have been used, including design variation, system achievement, materials, structure weight, control, and trajectory analysis. However, there were no clear descriptions of detailed aerodynamic performance, and at present there is no concrete design principle for winged flyback boosters.

Because space transport systems experience more severe flight conditions than those to which aircraft are exposed, the geometry of the winged flyback booster is highly constrained, with the wings having especially severe shape constraints. Nevertheless, the wing is the most important element for the flyback booster because it generates the aerodynamic performance. Therefore, the relationships among aerodynamic characteristics, such as lift, drag, and moment, are significant design information. It is important to find design variables sensitive to the aerodynamic performance; that is, acquisition of knowledge about the design space is essential to improve the aerodynamic performance of winged flyback boosters under severe shape constraints.

Received 17 November 2004; revision received 3 March 2005; accepted for publication 29 April 2005.

*Graduate Student, Department of Aeronautics and Space Engineering; currently Project Researcher, Japan Aerospace Exploration Agency. Member AIAA.
†Professor, Institute of Fluid Science. Associate Fellow AIAA.
‡Professor, Department of Aeronautics and Space Engineering. Associate Fellow AIAA.

In the present study, the wing shape of the TSTO RLV flyback booster was optimized with four objectives for aerodynamic performance. Based on the optimization results, tradeoff analysis was performed among the four objectives. By using a data-mining technique, design knowledge was obtained with regard to TSTO RLV winged flyback boosters.

II. Multiobjective Aerodynamic Optimization

A. Problem Definition

The reference mission of the TSTO RLV is to transport a 10-t payload into low earth orbit, similarly to the present H-IIA mission. The booster sizing is obtained by preliminary computation using the empirical equations developed by the Japan Aerospace Exploration Agency. Among the calculated geometrical data, the minimum fuselage diameter and the fuselage length are employed as constraints in the present optimization. This means that the fuselage geometry is fixed to a given size and only the wing shape is allowed to be optimized in the present parameterization system. The main reason for keeping the fuselage geometry fixed is that the fuselage is filled with the liquid-propellant rocket engines, so little change to its size is possible.

Trajectory analysis[5] around a typical TSTO configuration based on the present mission showed that the separation of the booster and orbiter takes place at roughly Mach 3. Then the flyback booster turns over, slows down, cruises at transonic speeds, and lands at subsonic speed. Note that the major part of its crossrange is in the transonic region. In the present study, the following four objective functions were considered:

Objective 1: Minimization of the shift of the aerodynamic center between supersonic and transonic flights:

$$F_1 = \left| C_{M_p}^{\text{supersonic}} - C_{M_p}^{\text{transonic}} \right| \tag{1}$$

A significant control problem related to the RLV flight may originate in the large variation of the aerodynamic center between supersonic and transonic flight conditions. Therefore, it is desirable to design wing shapes with less variation in the aerodynamic center, which will yield easier stability control.

Objective 2: Minimization of the pitching moment under the transonic flight conditions:

$$F_2 = \left| C_{M_p}^{\text{transonic}} \right| \tag{2}$$

The arrow wing ensures good aerodynamic performance, but it also produces a large pitching moment. Thus, it should be minimized under transonic flight conditions to achieve less trim drag and better flight stability.

Objective 3: Minimization of drag under the transonic flight conditions:

$$F_3 = C_D^{\text{transonic}} \tag{3}$$

Trajectory analysis showed that the range of the RLV booster is mostly covered by the transonic flight. Thus, the transonic drag should be minimized to increase the flight range.

Objective 4: Maximization of lift under the subsonic flight conditions:

$$F_4 = C_L^{\text{subsonic}} \tag{4}$$

To reduce the required runway distance, the lift obtained under subsonic flight conditions should be maximized.

B. Optimizer

In the present study, Adaptive Range Multi-Objective Genetic Algorithm (ARMOGA)[6] was used as an optimizer. ARMOGA is an efficient multiobjective evolutionary algorithm designed for aerodynamic optimization and multidisciplinary design optimization problems using high-fidelity computational fluid dynamics (CFD) solvers with large computational time. ARMOGA has range adaptation based on population statistics, and thus the population is reinitialized every N generations so that the search region adapts toward more promising regions. ARMOGA can be used to obtain nondominated solutions efficiently because of the concentrated search of the probable design space, and it also produces diversified solutions.

C. Aerodynamic Evaluation

In the present study, the unstructured mesh method[7] was used to evaluate aerodynamic performance. The three-dimensional Reynolds-averaged Navier–Stokes (RANS) equations are computed with a finite-volume cell-vertex scheme. The unstructured hybrid mesh method[8] is applied to capture the boundary layer accurately and efficiently. The Harten–Lax–van Leer–Einfeldt–Wada Riemann solver[9] is used for the numerical flux computations. The Venkatakrishnan's limiter[10] is applied when reconstructing second-order accuracy. The lower-upper symmetric Gauss–Seidel implicit scheme[11] is applied for time integration. For turbulence models, the Spalart–Allmaras one-equation model modified by Dacles-Mariani et al.[12] is employed without transition.

D. Geometry Definition

The design variables are related to planform, airfoil shape, wing twist, and position relative to the fuselage. A wing planform is determined by five design variables. A kink is placed on the leading edge. Airfoil shapes are defined at the wing root, kink, and tip using thickness distributions and camber lines. The thickness distributions are described by Bézier curves using 11 control points and linearly interpolated in the spanwise direction. The camber line distributions are parameterized using Bézier curves with four control points and incorporated linearly in the spanwise direction. Wing twist is refined using B-splines with six control points. The position of the wing root relative to the fuselage is parameterized by x and z coordinates of the leading edge, angle of attack, and dihedral angle. The entire wing shape is thus defined using 71 design variables. Once a wing is defined, the junction line between the wing and fuselage is extracted and the final wing–fuselage geometry is derived by neglecting part of the wing inside the fuselage.[13]

III. Optimization Results

As the population size was set to 8, the CFD preprocesses were parallelized on eight processing elements (PEs). Because a design candidate must be evaluated under three flow conditions, 24 RANS computations were needed in one generation. The population was reinitialized every five generations for range adaptation. First, evolutionary computation of 30 generations was performed. Then, the evolutionary operation was restarted using eight nondominated solutions extracted from all solutions of 30 generations, and 10 generations were computed. The total evolutionary computation of 40 generations was performed. Consequently, a total of 102 nondominated solutions extracted from all solutions of 40 generations were obtained for tradeoff analysis.

Figure 1 shows the two two-dimensional projections of the nondominated solutions to better understand the tradeoffs among the four objective functions. The optimum values of F_1 and F_2 are zero, and the nondominated solutions reached the origin, that is, the optimum values of F_1 and F_2 in Fig. 1a. Because the plots in Fig. 1a are the nondominated solutions for not two but four objective functions, there is a tradeoff surface spread of the nondominated solutions near the origin. Figure 1a shows that there is no tradeoff between the shift of aerodynamic center and the transonic C_{Mp}. The Pareto front can be seen clearly between F_3 and F_4 in Fig. 1b. Thus, Fig. 1b indicates that there is a marked tradeoff between the transonic drag and the subsonic lift. This result indicated that a high-lift

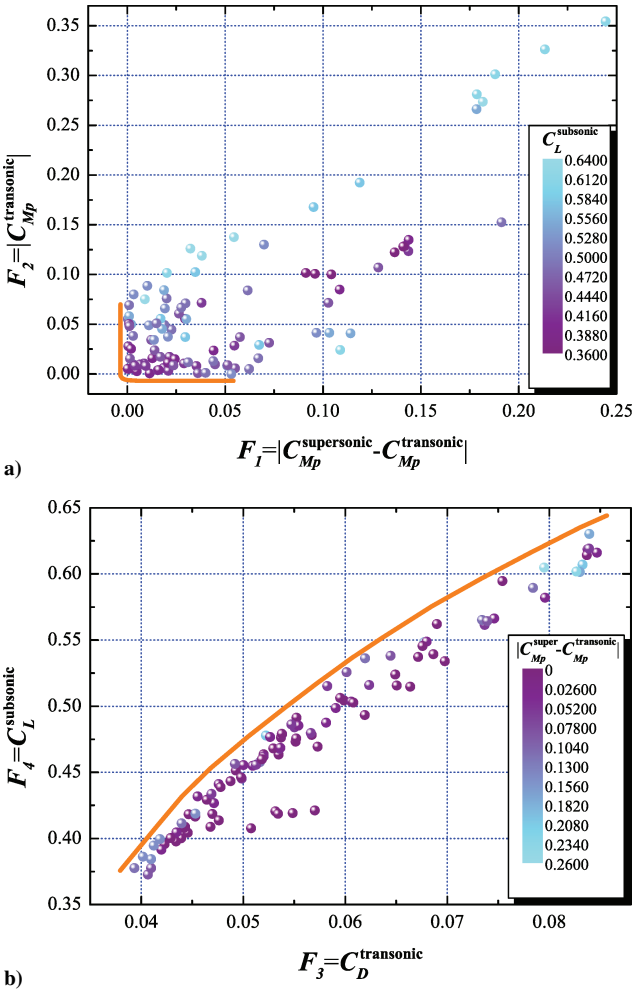

Fig. 1 Derived nondominated solutions on two-dimensional plane: a) between F_1 and F_2, and b) between F_3 and F_4.

device may be needed for an RLV booster for landing, similarly to aircraft. The Pareto front for F_2 attained the optimum front. However, the Pareto front for F_3 did not reach C_D of zero. Thus, there is a slight tradeoff between F_2 and F_3, and the transonic drag can be improved while the transonic C_{Mp} increases. Moreover, the Pareto front for F_1 attained the optimum front. However, the Pareto front for F_4 did not have an apparent limit. Therefore, there was a slight tradeoff between F_1 and F_4. This indicated that shift and transonic C_{Mp} were optimized simultaneously, while the subsonic lift was reduced slightly.

IV. Data Mining by Self-Organizing Map

If the optimization problem has only two objectives, tradeoffs can be visualized easily. However, if there are more than three objectives, a technique for visualizing the computed nondominated solutions is needed. Therefore, in the present study, self-organizing maps (SOMs), proposed by Kohonen,[14] were employed. SOMs are not only a technique for visualization but also a tool for the intelligent compression of information. That is, SOMs can be applied to data mining to acquire knowledge regarding the design space. In the present study, Viscovery SOMine[15] (Eudaptics GmbH, Austria) was employed.

A. Viscovery SOMine

Although SOMine is based on the SOM concept and algorithm, it employs an advanced variant of unsupervised neural networks, that is, Kohonen's Batch-SOM.

The algorithm consists of two steps that are iteratively repeated until no more significant changes occur. First the distances between all data items $\{\boldsymbol{x}_i\}$ and the model vectors $\{\boldsymbol{m}_j\}$ are computed and each datum $\boldsymbol{x}_i$ is assigned to the unit c_i that represents it best.

In the second step, each model vector is adapted to better fit the data it represents. To ensure that each unit j represents similar data to its neighbors, the model vector $\boldsymbol{m}_j$ is adapted not only according to the assigned data but also in regard to those assigned to the units in the neighborhood. The neighborhood relationship between two units j and k is usually defined by a Gaussian-like function,

$$h_{jk} = \exp\left(-d_{jk}^2 / r_t^2\right) \tag{5}$$

where d_{jk} denotes the distance between the units j and k on the map, and r_t denotes the neighborhood radius, which is set to decrease with each iteration t.

Assuming a Euclidean vector space, the two steps of the Batch-SOM algorithm can be formulated as

$$c_i = \arg\min \|\boldsymbol{x}_i - \boldsymbol{m}_j\| \tag{6a}$$

$$\boldsymbol{m}_j^* = \frac{\sum_i h_{jc_i} \boldsymbol{x}_i}{\sum_i h_{jc_i}} \tag{6b}$$

where $\boldsymbol{m}_j^*$ is the updated model vector.

In contrast to the standard Kohonen algorithm, which makes a learning update of the neuron weights after each record being read and matched, the Batch-SOM takes a "batch" of data, typically all records, and performs a collected update of the neuron weights after all records have been matched. This is much like epoch learning in supervised neural networks. The Batch-SOM is a more robust approach, because it mediates over a large number of learning steps. Most important, no learning rate is required. The SOMine implementation combines four enhancements to the plain Batch-SOM algorithm.[16] In SOMine, the uniqueness of the map is ensured by the adoption of the Batch-SOM and the linear initialization for input data.

Much like some other SOMs,[17] SOMine creates a map in a two-dimensional hexagonal grid. Starting from numerical multivariate data, the nodes on the grid gradually adapt to the intrinsic shape of the data distribution. Because the order on the grid reflects the neighborhood within the data, features of the data distribution can be read off from the emerging map on the grid.

In SOMine, the trained SOM is systematically converted into visual information. The tool provides an extensive built-in capability for both preprocessing and postprocessing as well as for the automatic color coding of the map and its components. SOMine is particularly useful in the determination of dependencies between variables, as well as in the analysis of high-dimensional cluster distributions.

B. Cluster Analysis

Once SOM projects input space anto a low-dimensional regular grid, the map can be utilized to visualize and explore properties of the data. When the number of SOM units is large, tofacilitate quantitative analysis of the map and the data, similar units need to be grouped, that is, clustered. The two-stage procedure—first using SOM to produce the prototypes which are then clustered in the second stage—was reported to perform well when compared to direct clustering of the data.[17]

Hierarchical agglomerative algorithm is used for clustering here. The algorithm starts with a clustering where each node by itself forms a cluster. In each step of the algorithm two clusters are merged: those with minimal distance according to a special distance measure, the SOM-Ward distance.[15] This measure takes into account whether two clusters are adjacent in the map. This means that the process of merging clusters is restricted to topologically neighboring clusters. The number of clusters will be different according to the hierarchical sequence of clustering. A relatively small number will be chosen for visualization, whereas a large number will be used for generation of codebook vectors for respective design variables.

C. Visualization of Design Tradeoffs

The resulting 102 nondominated solutions were projected onto the two-dimensional map of SOM. Figure 2 shows the SOMs colored by the four objective values, which have 10 clusters taking the four objective functions into considering. These color figures show that the SOMs can be grouped as follows: The upper center area on SOM corresponds to the designs with low shift of the aerodynamic center. The upper right corner corresponds to the designs with low shift of the aerodynamic center, transonic C_{Mp} and transonic C_D. The lower

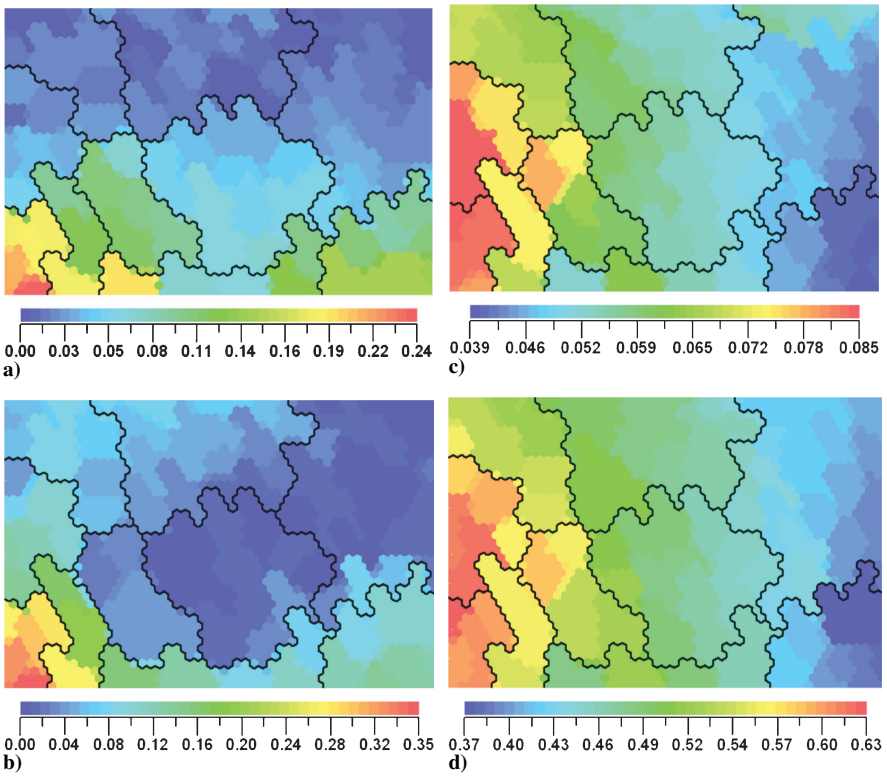

Fig. 2 SOM colored by each objective function: a) the shift of the aerodynamic center, b) the transonic C_{Mp}, c) the transonic C_D, and d) the subsonic C_L.

right corner corresponds to the designs with low transonic C_D. The lower left corner corresponds to high shift of the aerodynamic center, transonic C_{Mp} and transonic C_D. The left center region corresponds to high subsonic C_L.

The comparison between these colored SOMs reveals the tradeoffs and correlation between the objective functions. Figures 2a and 2b show high-value regions for the shift of aerodynamic center and the transonic C_D coincide with each other. That is, when one objective function is increased, another objective function is also increased strictly. Furthermore, because Fig. 2c is very similar to Fig. 2d, there is a severe tradeoff between transonic C_D and subsonic C_L because transonic C_D is minimized and subsonic C_L is maximized. This knowledge from SOM corresponds to the results of Fig. 1b.

D. Data Mining of Design Space

SOM can also be contoured by 71 design-variable values. Figure 3a shows the SOM colored by the design variable of the x coordinate of wing position to fuselage illustrated in Fig. 3b. Here, the x coordinate is held on the fuselage. Higher values are located in the lower left corner in Figs. 2a and 2b. High values of the shift of aerodynamic center, transonic C_{Mp}, and transonic C_D are clustered in this area. Thus, this means that the values of shift, transonic C_{Mp}, and transonic C_D become poorer when the wing position is behind the fuselage.

The SOMs colored by the other characteristic design-variable values indicate the following knowledge. An individual with lower rearward camber height at the wingtip has lower transonic C_D. An individual with higher rearward camber height at the kink has higher subsonic C_L.

When the sweepback angle of the inboard wing becomes larger, the inboard wing acts as a strake. In general, as a strake generates a vortex, it may be effective to increase lift due to leading-edge separation. However, the SOM colored by the design variable of the sweepback angle of the inboard wing shows that there are mixed values in the area in which high values of the subsonic lift are clustered. That is, the sweepback angle of the inboard wing is not effective to increase C_L. The CFD visualization, which is one individual under subsonic flow conditions where leading-edge separation is indicated by vortex centerlines, shows that the primary vortex occurs not from a strake but from a kink corner on the leading edge. Hence, the strake vortex is not essential to increase C_L. The knowledge for the CFD visualization is also obtained from SOM.

Because the SOMs colored by several other design variables had jumbled coloring, their design variables had no effect in determining tradeoffs among the four objective functions. That is, the sorting of the design variables can also be performed from SOM.

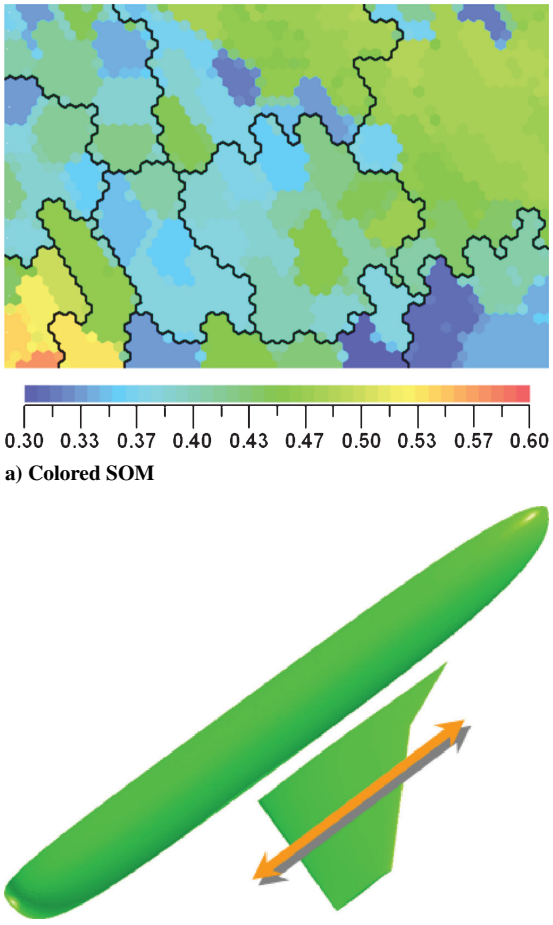

a) Colored SOM

b) Sketch

Fig. 3 Design variable regarding x-axis of wing position to fuselage.

V. Conclusion

The wing for a TSTO RLV flyback booster powered by a liquid-propellant rocket engine for VTHL was optimized by considering four aerodynamic objective functions using ARMOGA. Consequently, the tradeoff information among the four objective functions has been revealed. No tradeoff exists between the shift of aerodynamic center and transonic pitching moment. However, a severe tradeoff was found between transonic drag and subsonic lift.

Moreover, data mining for the design space was performed using SOM. For example, wing position should not be too far to the rear of the fuselage, to decrease the shift in the aerodynamic center between supersonic and transonic flow conditions, transonic pitching moment, and transonic drag. Rearward camber height at the tip has an influence on transonic drag. Rearward camber height at the kink increases subsonic lift. Strake has less effect on the increase in subsonic lift and primary leading-edge separation from the outboard wing is more important for vortex lift. Data mining provides knowledge regarding the design space, which is considered an important facet of solving optimization problems.

Acknowledgment

The present computation was carried out using the supercomputers NEC SX-5 and SGI ORIGIN2000 in the Institute of Fluid Science, Tohoku University.

References

[1]Andrews, J., and Andrews, D., "Low Cost Options for 2nd and 3rd Generation Reusable Launch Vehicles," AIAA Paper 00-3824, July 2000.

[2]Powell, R. W., Lockwood, M. K., and Cook, S. A., "The Road from the NASA Access-to-Space Study to a Reusable Launch Vehicle," IAF-98-V.4.02, 1998.

[3]Tartabini, P. V., Wurster, K. E., Korte, J. J., and Lepsch, R. A., "Multidisciplinary Analysis of a Lifting Body Launch Vehicle," *Journal of Spacecraft and Rockets*, Vol. 39, No. 5, 2002, pp. 788–795.

[4]Naftel, J. C., and Powell, R. W., "Analysis of the Staging Maneuver and Booster Glideback Guidance for a Two-Stage, Winged, Fully Reusable Launch Vehicle," NASA TP-3335, April 1993.

[5]Iwata, T., Sawada, K., and Kamijo, K., "Conceptual Study of Rocket Powered TSTO with Fly-Back Booster," AIAA Paper 2003-4813, July 2003.

[6]Sasaki, D., and Obayashi, S., "Efficient Search for Trade-Offs by Adaptive Range Multi-objective Genetic Algorithms," *Journal of Aerospace Computing, Information, and Communication*, Vol. 2, No. 1, 2005, pp. 44–64.

[7]Ito, Y., and Nakahashi, K., "Direct Surface Triangulation Using Stereolithography Data," *AIAA Journal*, Vol. 40, No. 3, 2002, pp. 490–496.

[8]Ito, Y., and Nakahashi, K., "Improvements in the Reliability and Quality of Unstructured Hybrid Mesh Generation," *International Journal for Numerical Methods in Fluids*, Vol. 45, No. 1, 2004, pp. 79–108.

[9]Obayashi, S., and Guruswamy, G. P., "Convergence Acceleration of an Aeroelastic Navier–Stokes Solver," *AIAA Journal*, Vol. 33, No. 6, 1994, pp. 1134–1141.

[10]Venkatakrishnan, V., "On the Accuracy of Limiters and Convergence to Steady State Solutions," AIAA Paper 93-0880, Jan. 1993.

[11]Sharov, D., and Nakahashi, K., "Reordering of Hybrid Unstructured Grids for Lower-Upper Symmetric Gauss–Seidel Computations," *AIAA Journal*, Vol. 36, No. 3, 1998, pp. 484–486.

[12]Dacles-Mariani, J., Zilliac, G. G., Chow, J. S., and Bradshaw, P., "Numerical/Experimental Study of a Wingtip Vortex in the Near Field," *AIAA Journal*, Vol. 33, No. 9, 1995, pp. 1561–1568.

[13]Sasaki, D., Yang, G., and Obayashi, S., "Automated Aerodynamic Optimization System for SST Wing-Body Configuration," *Transactions of the Japan Society for Aeronautical and Space Sciences*, Vol. 46, No. 154, 2004, pp. 230–237.

[14]Kohonen, T., *Self-Organizing Maps*, Springer-Verlag, Berlin/Heidelberg, 1995.

[15]*Eudaptics Web site*, URL: http://www.eudaptics.com [cited 16 June 2004].

[16]Deboeck, G., and Kohonen, T., *Visual Explorations in Finance with Self-Organizing Maps*, Springer Finance, London, 1998.

[17]Vesanto, J., and Alhoniemi, E., "Clustering of the Self-Organizing Map," *IEEE Transactions on Neural Networks*, Vol. 11, No. 3, 2000, pp. 586–600.